Prediction of surface roughness and porosity in SLM-fabricated SS316L components using an artificial neural network approach

Amit Sharma[1,*], *Tauseef* Uddin Siddiqui[2], *Manoj* Kumar Singh[1], *Anil* Kumar Bisht[3], *Arshad* Noor Siddiquee[2], and *Shwetank* Avikal[4]

[1]Department of Mechanical Engineering, Faculty of Engineering & Technology, M.J.P. Rohilkhand University, Bareilly, India
[2]Department of Mechanical Engineering, Faculty of Engineering & Technology, Jamia Millia Islamia, New Delhi, India
[3]Department of CSIT, Faculty of Engineering & Technology, M.J.P. Rohilkhand University, Bareilly, India
[4]Department of Management Studies, Graphic Era University, Dehradun, India

Abstract. Selective Laser Melting (SLM) is a sophisticated additive manufacturing process utilizing a high-energy laser to selectively melt layers of metallic powder according to a CAD design. The online monitoring and control of defects is a challenging task in SLM fabrication which is necessary to maintain the functionality and longevity of parts. No universally accepted model has been developed, for prediction of surface defects and porosity in SLM-fabricated parts. Image processing using artificial neural networks (ANN) has been successfully used in various fields such as in quality control, human computer interaction, remote sensing, and construction. In this paper, ANN model was utilized for estimation of porosity and surface roughness (R_a) of SLM-fabricated components. The SEM images were used as input for pattern extraction by image processing using ANN model. The integrity of the ANN model to predict the optimum process parameters for the minimum R_a and porosity was assessed. Both testing as well as training data sets showed lower values of the mean absolute error (MAE) & mean square error (MSE) at 0.9662 and 1.6296, indicating a well-trained ANN model. 2.45% and 3.07% average error was obtained between actual and predicted values of R_a and porosity. This research has developed a fast and accurate method for prediction of R_a and porosity to improve functionality and longevity of SLM-fabrication components.

1 Introduction

In additive manufacturing (AM), wire or powder is used as substrate, melted by a concentrated heat source, and then consolidated to create components. With the use of 3D model data, it is possible to fabricate a variety of structures and intricate geometries,

* Corresponding author: sharma_amit0408@yahoo.com

providing a large selection of goods and custom-specification alternatives without incurring any fabrication cost penalties[1]. SLM, a metal additive manufacturing (MAM) method, is typically used for high-end expensive parts with limited manufacturing capacity, excellent precision, and outstanding mechanical properties. The stainless steel (SS) of SS316L specification is a low-carbon austenitic SS with excellent printability in MAM. SS 316L is widely employed in biomedical applications due to its excellent biocompatibility, in marine, chemical, and pharmaceutical industries because of high corrosion resistance and in aerospace and automobile due to its suitable mechanical properties[2].

Gu et al. [3]concluded that low laser power led in coarsened balls with structural fragility, whereas high scan speed produced micrometer-scaled balls due to laser-induced melt splashes. Increasing input energy density could reduce balling, which led to reduced surface roughness. Yadroitsev et al.[4] studied SLM behavior of different grades stainless steel and concluded the fact, stability regions and instability zones in metal powder production, with distortions and abnormalities at low scanning speed and balling effects at high speeds. Yang et al. [5] investigated impact of linear energy density (LED) upon vertical plane R_a .They showed that the R_a reduced from 15 μm to 4 μm, with a reduction of almost 70% when a suitable LED was used. R_a was greatly impacted by the deposited tracks' surface morphologies and height change rates, and under the same LED settings, R_a was even more reduced at increased laser power. Charles et al. [6] emphasized the significance of volumetric energy density (VED) in assessing down-facing surfaces and concluded that greater dimensional deviations and reduced roughness were the results of increasing VED and R_a at multiple down-facing inclined layers. The 'inverse mushroom' artifacts in 'Low VED' mode caused surface roughness to increase, whereas 'High VED' mode produced larger, coalescent meltpool that producd smoother, less rough surfaces. Manikandan & Venkatesan [7] investigated that increased VED significantly reduced surface roughness on the top surface (PPBD), with R_a values of 8.1 μm at 79 J/mm³ and 25.4 μm at 35 J/mm³. However, the side surface (PBD) showed variable R_a values, ranging from 4.26 μm at 52 J/mm³ to 18.64 μm at 60 J/mm³. Their study showed that surface orientation, laser power, and scanning speed had a significant impact on surface finish quality.

Surface roughness strongly influences the quality as well as functional performance of the additively manufactured components, it is a major problem when SLM-fabricated SS316L components employs at high end applications. The staircase effect, which is especially noticeable on curved and sloped surfaces, is caused by the natural layer-wise manufacturing process. Increased surface imperfections are also a result of partially melted powder particle adhesion, poor laser parameters, melt pool instability, and build orientation. As-built surface roughness values typically range from 5–10 μm on top surfaces and can exceed 25 μm on side or inclined surfaces in contrast to 1-2 μm in mechanical processed like grinding, machining along with milling[8]. These surface features degrade the fatigue strength, corrosion resistance, dimensional correctness, and overall aesthetic quality of the components. Rough surfaces can act as initiation sites for crack propagation under cyclic loads or promote localized corrosion in harsh settings due to micro-crevices. Meeting the rigorous surface quality requirements in critical applications requires optimizing process parameters.

Yusuf et. al. [9] investigated that with an average porosity of nearly 0.82%, the SLM-built 316L stainless steel samples attained densification of nearly 99%. However mechanical characteristics of SLM-fabricated SS 316L samples were not considerably impacted by this low porosity. Barrionuevo et. al.[10] concluded that porosity levels in SLM-fabricated parts of SS316L was directly impacted by scanning speed. A VED of 125 J/mm³ was required to attain maximal relative density and avoid fusion mistakes. Scanning speed had the biggest impact on relative density and microhardness. Porosity values (< 1%)

that were comparable to those obtained using conventional techniques, demonstrating SLM's applicability in the production of mechanical components.

Few studies have been conducted in the past on porosity determination by image processing techniques and ANN. Alamri et al. [11]developed a method for prediction of porosity in CT images of SLM fabricated parts using Convolutional Neural Network (CNN). The prediction accuracy for porosity increased from 68.60% to 75.50% with the use of this CNN model. Pandelea et al.[12] used ANN model for image processing, date reduction, segmentation and recognition. These images can be represented as a matrix of elements which consists of colour information for each pixel. This matrix is used as input data into the ANN model. Soler et al. [13] used ANN model for prediction of R_a in SLM fabricated parts after blasting and electro polishing. The optimum settings were achieved to obtain minimum R_a with a reduction of 60%.

It was found from literature review that an abundance of effort has not been executed on prediction of surface quality of SLM fabricated parts of SS316L alloy using image processing by ANN model. No universally accepted model has been developed, for prediction of surface defects and porosity in SLM fabricated parts. The visual images are used as input for pattern extraction using image processing by ANN model. This model is employed to conduct classification tasks for prediction of R_a and porosity (%) in SLM fabricated parts. Porosity mapping was also determined to identify and classify regions of key holes, gas porosity and lack of fusion in SLM fabricated parts under different process conditions.

2 Materials and methods

2.1 Powder material

Austenite stainless steel metallic powders (particles size = 15-60 μm) of grade SS316L (Cr=17.7, Ni=12.7, Mo=2.36, Mn=0.65, Si=0.62, O=0.03, C=0.022, Cu=0.02, Fe=Balanced) was utilized for fabrication of samples. This alloy is useful in aerospace, automotive, pharmaceutical, biomedical, marine, chemical and food industry because of its exceptional mechanical characteristics, biocompatibility, resistance to corrosion, aggressive environment and non-toxic behaviour[14].

2.2 Experimental work

SLM 280 metal printer [Make: SLM Solutions, Germany; Power: 400W; Build Envelope: 280 x 280 x 365mm³] was utilized to fabricate cylindrical components with diameter 10 mm and height 5.0 mm, as illustrated in Figure 1. This metal printer was equipped with fiber laser. The diameter of laser beam was 80 μm. The range of process parameters (Laser power=250, 300, & 350 Watt; Scan Speed=700, 800, & 900 mm/sec and Hatch distance=0.11, 0.12, & 0.13mm) for conducting experimental work was decided according to available literature. To optimize fabrication process, the thickness of each layer remained consistent (=30 μm). The "L_{27} Taguchi design of experiment" technique was applied for conducting experiments under different process settings of SLM using SS316L powder. Electric discharge machining was applied for removal the prepared samples from the base of the SLM machine. The volumetric energy density (VED) for various sets of process-related variables was determined employing the following equation:

$$\mathrm{VED} = \frac{\mathrm{P}}{\mathrm{S}\times\mathrm{H}\times\mathrm{T}} \quad (1)$$

Here P stands for laser power, S for scanning speed, H for hatch spacing and T for layer thickness. Electric discharge machining was used to cut the fabricated samples from the build plate of the SLM metal printer. Build platform and build direction of SLM fabricated parts is illustrated by Figure 2.

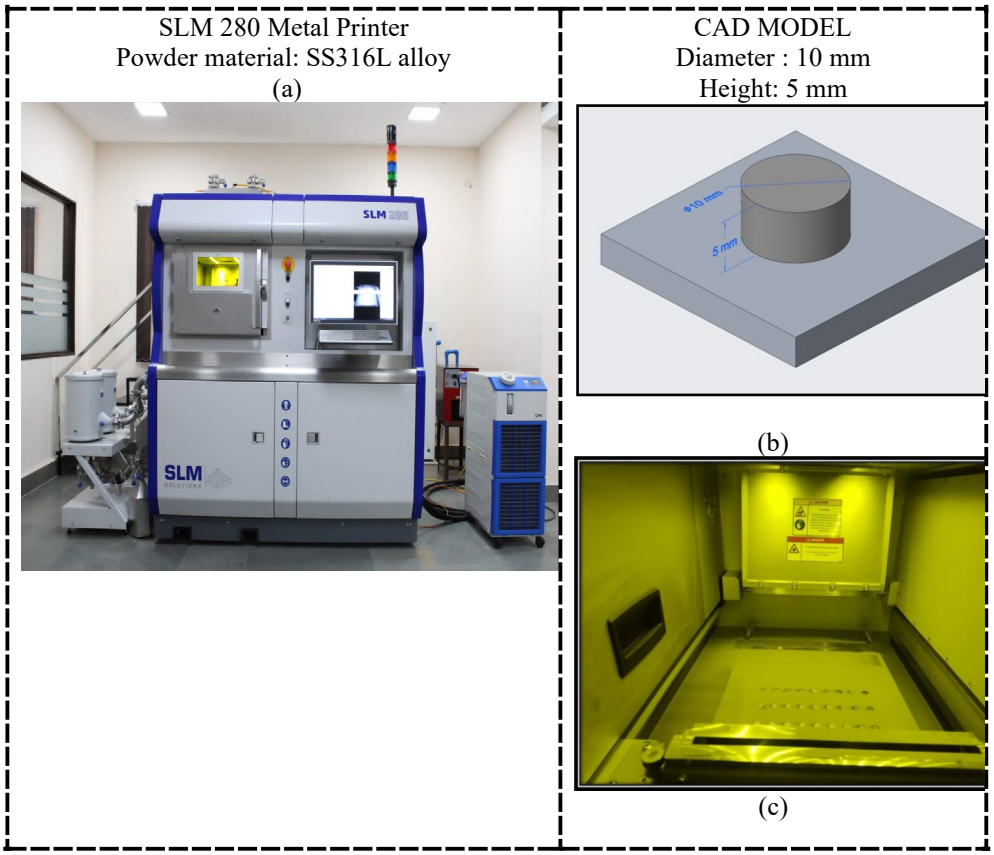

Fig. 1. (a) SLM 280 metal printer (b) CAD model, and (c) SLM Fabricated parts.

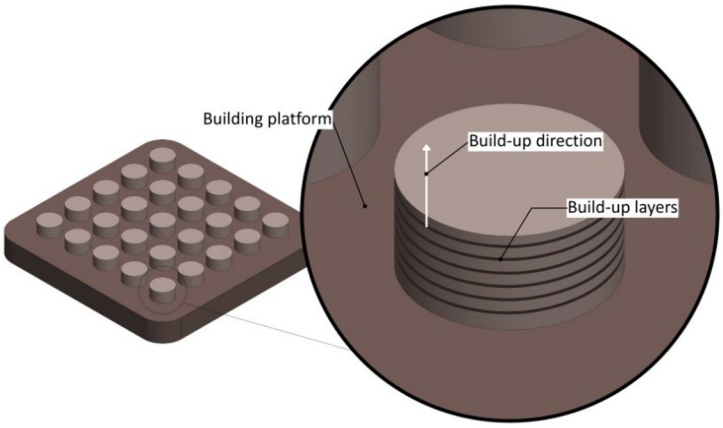

Fig. 2. Build platform and build direction of SLM fabricated parts.

2.3 Measurement of surface roughness

Surface roughness (R_a) in SLM-fabrication is the combined effect of incomplete melting of powder particles, melt pool dynamics and layer by layer build process. This R_a can significantly impact the performance and quality of 3D printed parts. It can affect wear resistance, fatigue performance, corrosion resistance and dimensional tolerance of SLM fabricated parts. The Mitutoyo SJ-201 [Make: Mitutoyo Corporation, Japan; Model: Surftest SJ-201], depicted in Figure 3, was used for the surface roughness measurement of SLM-fabricated samples. To eliminate error and improve measurement precision, every measurement was conducted three times, and the mean result was used for consideration.

Fig. 3. Measurement of R_a of SLM fabricated parts.

2.4 Porosity mapping

Porosity in SLM arises from issues related to powder characteristics, energy input and process parameters. Two primary sorts of pores were analysed: Spherical pores due to entrapped gas and irregular pores as consequence of lack of fusion. These defects might have substantial effects on the mechanical characteristics, surface integrity, as well as functional qualities of SLM-fabricated samples. The porosity was determined in SLM-fabricated specimens using image segmentation, and classification by ANN model. The porosity (%) is determined using the following expression:

$$\text{Porosity (\%)} = \frac{\text{Total Pore Area}}{\text{Total Area}} \text{x} 100 \qquad (2)$$

2.5 Image processing by ANN model

ANN processes images through multiple layers that detect features like edges, shapes and textures. In SLM technique, ANN is used for image processing to improve part quality and process control. This ANN model will help to analyse SEM images of the SLM-fabricated samples to detect defects, classify melt pool characteristics, and potentially adapt the process parameters. This will results in superior product quality, process optimization, minimized waste, along with enhanced production efficiency during SLM fabrication of SS316L alloy.

In image processing, ANN provide a number of benefits, including as enhanced object recognition efficiency and accuracy, flexibility in handling complicated datasets, and the capacity to analyze big, high-resolution images. In this ANN model input layers extracted image features from SEM images through feature extractor and send it to first hidden layer. First hidden layer captured non-linear relations between SEM texture and porosity/surface roughness. On the basis of first hidden layer input, second hidden layer

further abstracted morphological features for porosity and roughness measurement. The third hidden layer worked on dimensionality reduction and mapping to regression space. The final output layers generated the ANN model's outcome of porosity and R_a. In this model, the input characteristics were standardized utilizing the MinMaxScaler. This scaled the values between 0 and 1. The dataset was divided into two set , 80% training & 20% testing data.

These images can be represented as a matrix of elements which consists of colour information for each pixel. This matrix is used as input data into the ANN model. The small dimension images can easily and quickly learn to identify the size and the quantity of input vectors[11]. Loss Function is taken as MSE, used for regression tasks. MAE, which helps to interpret performance. Adaptive Moment Estimation technique was adopted as optimizer. The ANN model was instructed for 100 epochs. It used validation data to monitor performance on unseen data and evaluates the model on test data. This trained model may be accurately employed to predict R_a for new SLM parameters. The ANN model used for prediction of R_a along with % porosity is depicted in Figure 4.

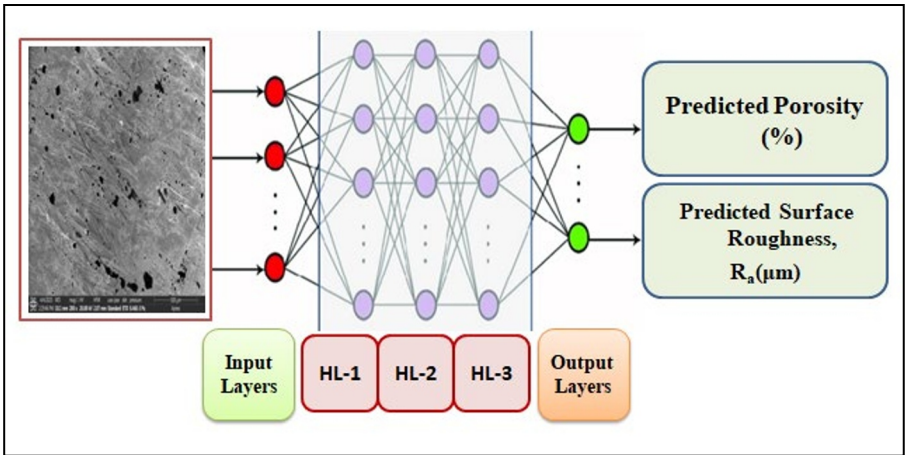

Fig. 4. ANN model used for prediction of surface roughness and porosity mapping.

2.6 Computation of ANN model

An artificial neural network (ANN) generates predictions for a given input throughout the training and evaluation stages. After comparing these predictions with the known actual values, the error is quantified by calculating the MAE, MSE, and coefficient of determination (R^2). The back propagation method then uses this error to modify the weights and biases of the network in an effort to reduce the error and increase prediction accuracy.

$$MAE = \frac{1}{N}\sum_{i=1}^{N} | y_i - \hat{y} | \quad (3)$$

$$MSE = \frac{1}{N}\sum_{i=1}^{N} (y_i - \hat{y})^2 \quad (4)$$

$$R^2 = 1 - \frac{\sum (y_i - \hat{y})^2}{\sum (y_i - \bar{y})^2} \quad (5)$$

where, y_i is the actual value, $\hat{y}$ is the predicted value and $\overline{y}$ is mean value of noticed responses i.e. surface roughness and % porosity of SLM-fabricated components.

3 Results and discussion

3.1 Comparison of actual and predicted surface roughness

The various images of SLM fabricated parts have been captured under different process settings using scanning electron microscope (SEM). These images are used as input for pattern extraction by image processing using ANN model as shown in Figure 5. This model is employed to conduct the classification tasks for prediction of R_a values in SLM fabricated parts. To train the ANN model, 80 % data sets were randomly chosen for the prediction of R_a values. Rest 20% data sets are used for testing and validation of the ANN model. The results obtained for prediction of R_a and porosity (%) value is summarized in Table 1. Figures 6 and 7 shows the variation of MAE and MSE values for training and validation data sets in ANN modeling. The model is trained for 100 epochs. It uses validation data to monitor performance on unseen data and evaluates this model on test data. Table 2 shows the error metrics and accuracy of ANN model in terms of average values of MAE and MSE after training and validation. The MAE and MSE values were found to be 0.9662, 1.6296, respectively which is fairly good indicating well trained ANN model.

This ANN model can be effectively implemented to accurate predicts R_a values for unknown database of SLM parameters. Since the predicted R_a values were closely aligned with the actual values, with coefficient of determination (R^2) obtained as 0.9473. Minor deviations from the best line of fit indicate small prediction errors. All the points lie on the best line of fit, the model's predictions match the actual values very well, indicating high prediction accuracy of 93.58% for R_a values as depicted in Table 2. The actual and predicted R_a values for different process settings have been shown in Figure 8. 2.45% error is obtained in the actual and predicted R_a values, using ANN model. At higher VED, surface disturbances in the melt pool may have negative effect on R_a. This can lead to keyhole formation, which are cylindrical holes that appear during SLM due to material vapor pressure within the melt pool. In the same manner, higher laser intensity may cause significant material vaporization along with recoil pressure, which may destabilize the melt pool and an increase in R_a[15]. The optimum settings for minimum R_a (9.504 μm) was obtained at low laser power, high scan speed, and low hatch distance.

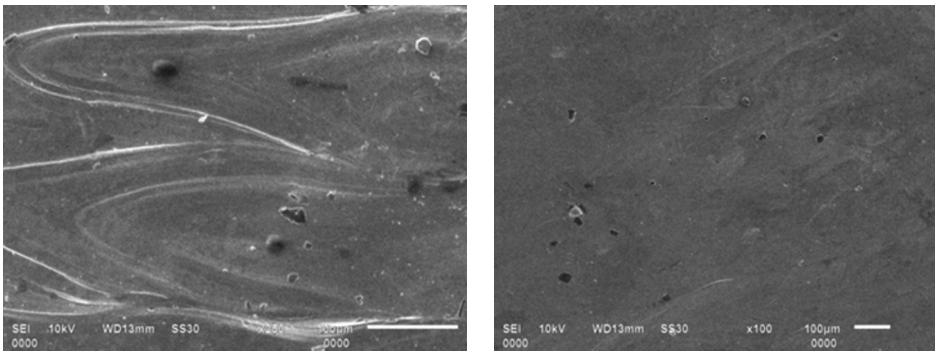

(a) (b)

Fig. 5. SEM images (a) Micrograph 1, and (b) Micrograph 2 for R_a.

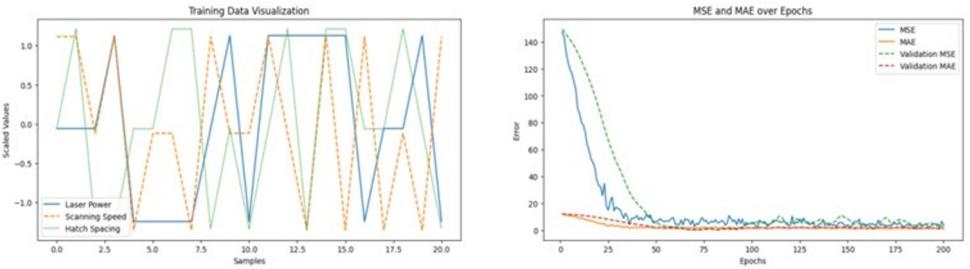

(a) (b)

Fig. 6. (a) Training data sets (b) MSE and MAE for traning and validation data sets for micrograph 1.

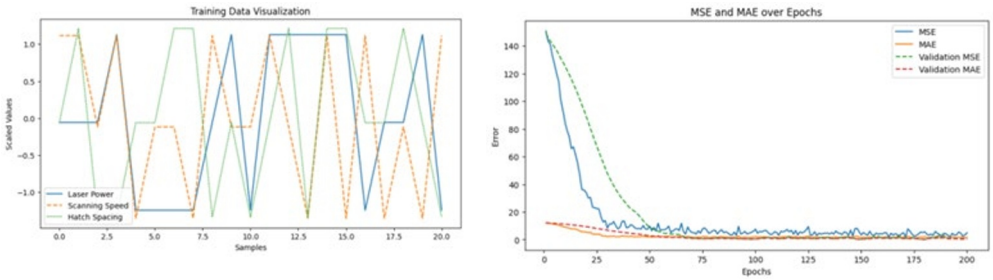

(a) (b)

Fig. 7. (a) Training data sets, and (b) MSE and MAE for traning and validation data sets for micrograph.

Table 1. Actual and Predicted R_a and Porosity (%) using ANN model.

S No.	SLM parameters			VED (J/mm^3)	Actual		Predicted	
	Laser power (W)	Scan speed (mm/s)	Hatch spacing (mm)		R_a (µm)	Porosity (%)	R_a (µm)	Porosity (%)
1	250	700	0.11	108.225	11.82	0.2466	11.704	0.2432
2	250	700	0.12	99.206	11.834	0.715	11.725	0.697
3	250	700	0.13	91.575	11.954	0.912	11.800	0.864
4	250	800	0.11	94.697	10.075	0.889	10.260	0.872
5	250	800	0.12	86.806	10.405	0.9277	10.398	0.9265
6	250	800	0.13	80.128	10.524	0.997	10.513	0.987
7	250	900	0.11	84.175	9.405	0.821	9.504	0.789
8	250	900	0.12	77.160	9.587	1.009	9.600	0.965
9	250	900	0.13	71.225	9.705	1.116	9.708	0.968
10	300	700	0.11	129.870	12.901	0.767	12.807	0.748

11	300	700	0.12	119.048	12.236	0.605	12.518	0.593
12	300	700	0.13	109.890	12.687	0.2121	12.727	0.230
13	300	800	0.11	113.636	12.645	0.3857	12.725	0.3624
14	300	800	0.12	104.167	12.806	0.425	12.721	0.413
15	300	800	0.13	96.154	12.85	0.814	12.882	0.756
16	300	900	0.11	101.010	13.349	0.511	13.349	0.487
17	300	900	0.12	92.593	13.492	0.902	13.409	0.887
18	300	900	0.13	85.470	13.597	0.881	13.524	0.864
19	350	700	0.11	151.515	13.852	0.9277	13.759	0.914
20	350	700	0.12	138.889	13.865	0.823	13.765	0.795
21	350	700	0.13	128.205	13.932	0.721	13.807	0.653
22	350	800	0.11	132.576	13.646	0.782	13.623	0.773
23	350	800	0.12	121.528	13.684	0.676	13.685	0.664
24	350	800	0.13	112.179	13.745	0.2493	13.685	0.234
25	350	900	0.11	117.845	12.934	0.5605	12.977	0.548
26	350	900	0.12	108.025	12.965	0.3248	13.003	0.3184
27	350	900	0.13	99.715	12.986	0.605	13.045	0.594

Table 2. Error metrics and prediction accuracy of ANN model.

Average R^2	**Average MAE**	**Average MSE**	**Average prediction accuracy (%)**
0.9473	0.9662	1.6296	93.58

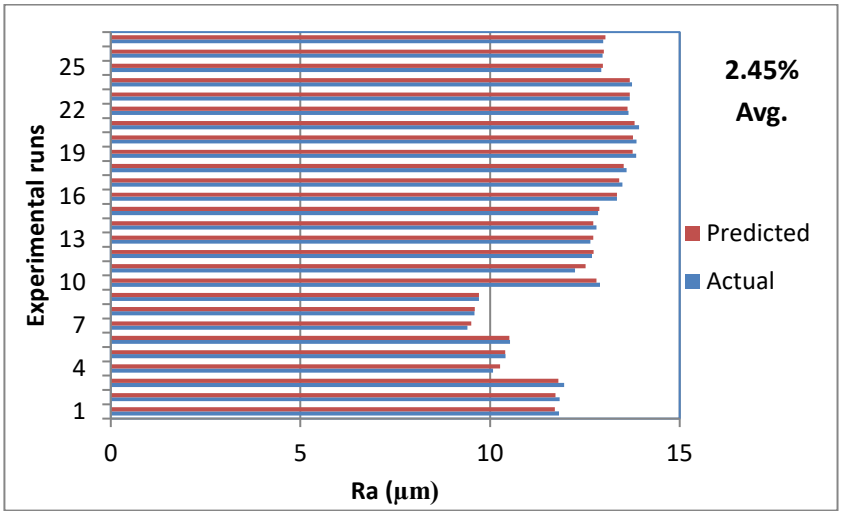

Fig. 8. Actual and predicted R_a values using ANN model.

3.2 Correlation heatmap

The correlation heatmaps are a graphical aid used in ANN models which displays the correlation among numerous factors in the colored matrix form. It illustrates the close relationship between many factors, much like a color chart. Finding patterns and relationships between variables in their data, as well as determining which variables may potentially lead to multi collinearity, are helpful. There was an inverse relationship between scanning speed and R_a, as seen in Figure 9, although laser power had a significant positive linear relationship with R_a. R_a and hatch spacing had little or no association, indicating that hatch distance had negligible effect on the surface quality during SLM fabrication of SS316 alloy.

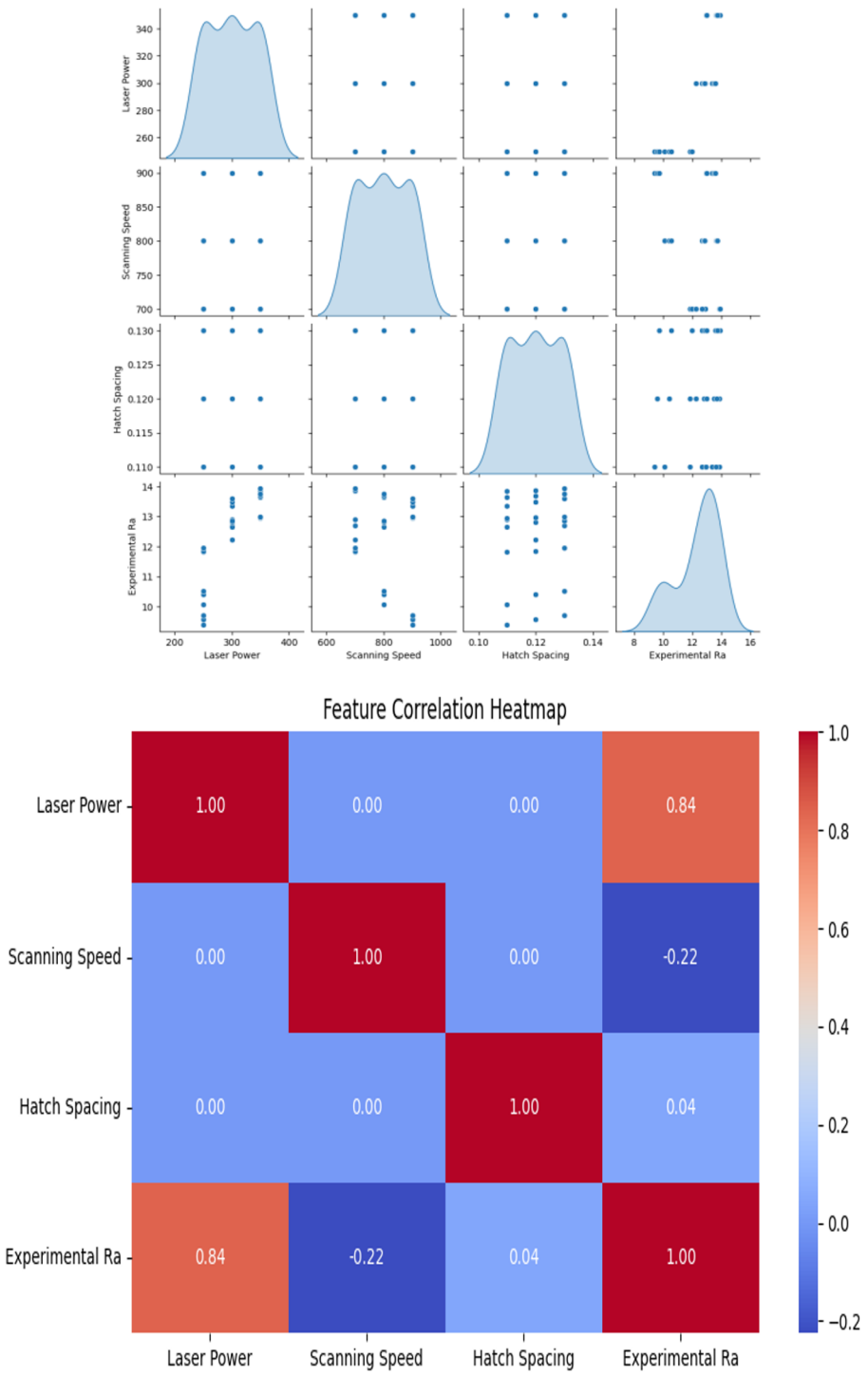

Fig. 9. Feature Correlation heatmap for R_a.

3.3 Porosity mapping using ANN model

The SEM images taken were utilized for image processing by ANN model to identify regions of porosity at different process settings as shown in Figures 10 and 11. This ANN model can be effectively utilized to conduct the classification tasks for identification and characterization of porosity in SLM-fabricated components. To train the ANN model, 80% data sets were randomly chosen for the prediction of porosity values. Rest 20% data sets were used for testing and validation of the ANN model. Selection of optimum process conditions can help reduce porosity defects and improve quality of the SLM fabricated parts. Due to lower VED, irregular porosities arise due of inadequate layer bonding and pockets of the unfused powder. The porosity, due to lack of fusion, decreased with an increase in VED values. The keyhole porosity was due to formation of high energy deep melt pool which increased with rise in VED value[2]. Additionally, it was noticed that the porosity of the feedstock was linked to the porosity of entrapped gases.

Spherical shaped pores of size 5-10 μm is observed due to gas entrapment within the powder particles. Keyhole porosity arises at high VED values due to formation of keyholes in deep melt pool as shown in Figure 12. The gas atomization of SS316L particles led to most of the pores getting spherical in appearance[9]. The porosity may also be observed due to excess energy supply during SLM process resulting in spatter ejection. The porosity in SLM-fabricated components was observed to be less than 1% which is better than the conventional manufacturing methods. The actual as well as predicted porosity for all process settings had been shown in Figure 13. 3.07% error was obtained in the prediction of porosity values with respect to actual porosity, by this ANN model. The maximum porosity in specimens was observed as 0.987% associated with VED of 80.128 J/mm^3. The minimum porosity determined in specimen was mapped to be 0.230% associated with VED of 109.89 J/mm^3.

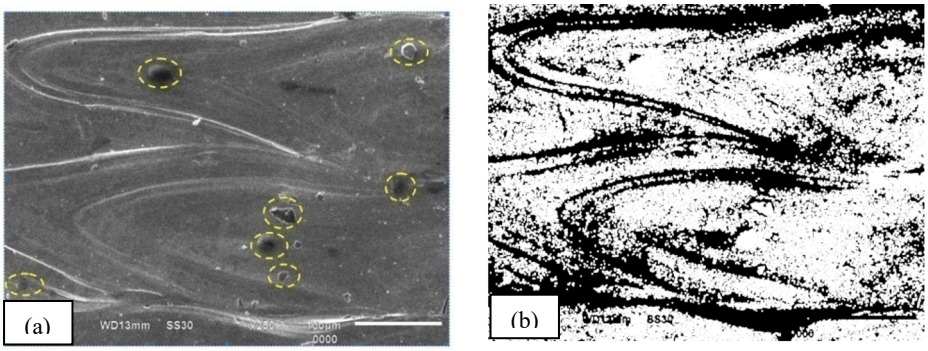

Fig. 10. (a) Porosity images, and (b) Image processed by ANN.

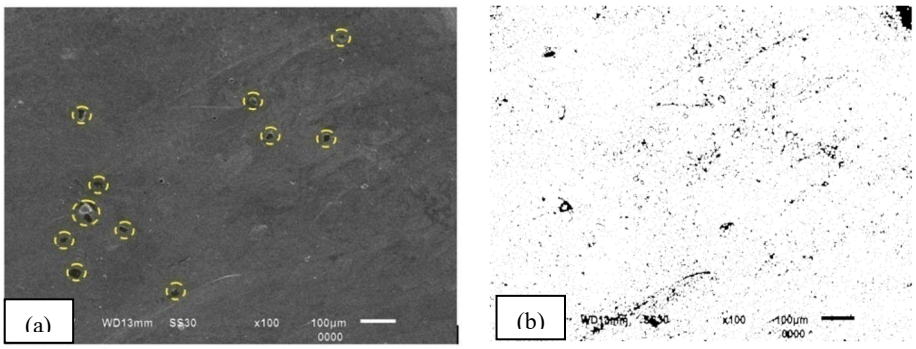

Fig. 11. (a) Porosity images, and (b) Image processed by ANN.

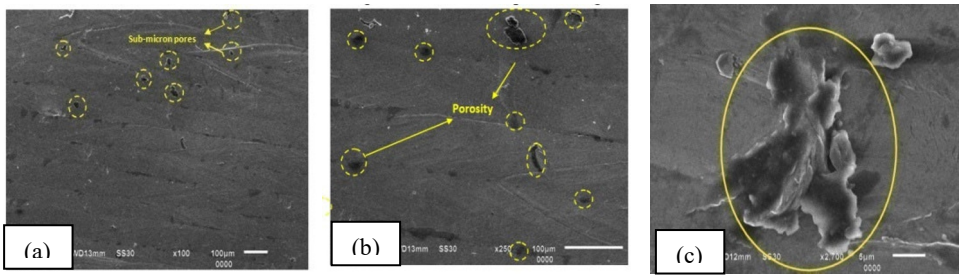

Fig. 12. Porosity images (a) Pore size 5-10µ, (b) Pore size 10-25µ, and (c) Pore size > 40µ.

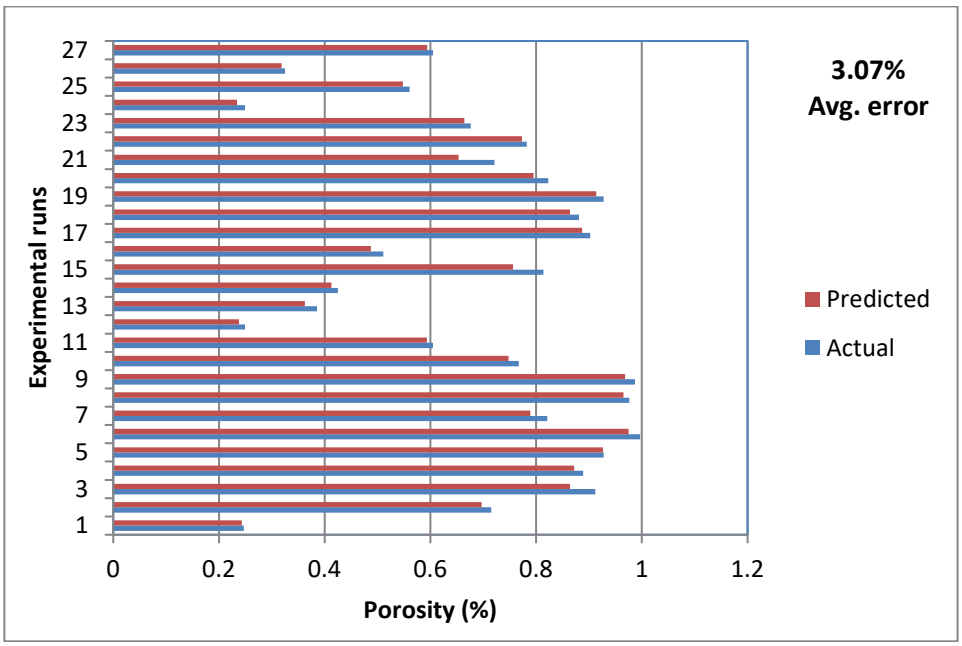

Fig. 13. Actual and predicted porosity (%) using ANN model.

4 Conclusion and future scope

The ANN based image processing technique is used to predict the R_a and % porosity in SLM-fabricated components, leading to better longevity as well as functionality. The visual

images are used as input for pattern extraction by image processing using ANN model. This model is employed to conduct the classification tasks for recognition as well as characterization of the imperfection in SLM-fabricated components. The following findings have been obtained from the current research:

- The ANN model's potential to precisely predict the optimum process parameters for the minimum R_a was assessed.
- The training and validation data sets yielded lower values of MAE and MSE as 0.9662 and 1.6296, indicating a well-trained ANN model.
- R_a values are predicted accurately by the ANN model with an accuracy of 93.58%.
- 2.45% and 3.07% average error is obtained between actual and predicted R_a and porosity values using ANN model.
- From the correlation heatmap, It was evident that laser power had strong correlation with R_a values as compared to other parameters.
- The optimum settings for minimum R_a (9.504 μm) was achieved at low laser power, high scan speed and low hatch distance.
- The highest and lowest R_a in SLM-fabricated components was observed to be as 13.807μm and 9.504 μm at VED value of 128.205 J/mm^3 and 84.175 J/mm^3.
- The porosity due to lack of fusion decreased with the increment in VED values.
- The keyhole porosity was as result of high energy deep melt pool which increases with increase in VED value.
- The highest and lowest porosity predicted in SLM-fabricated components by ANN model is as 0.987% and 0.230% at VED value of 80.128 J/mm^3 and 109.89 J/mm^3.
- The porosity of SLM-fabricated components was reported to be less than 1% which is better than the conventional fabrication methods.
- The ANN is superior for automatic extraction of intricate features without manual engineering leading higher accuracy and low cost in image processing as compared to CNN and SVM methods.
- These ANN predicted results can improve process monitoring and control, reduce defects and will improve part quality during real production.

Funding
No funding was received for this work.
Availability of data
The data of this study are available to from the corresponding author upon reasonable request.
Author contributions
A.S.: conceptualization, formal analysis, methodology, investigation, resources and writing—original draft; T.U.S: formal analysis, investigation, writing—review and editing, supervision and validation; M.K.S.: investigation, writing—review and editing, supervision and validation; A.K.B.: formal analysis, methodology, software, investigation, resources; A.N.S.: supervision, methodology, writing—review and editing, and validation; S.A.: methodology, formal analysis, investigation, resources and writing—original draft

References

1. A. Aversa, A. Saboori, G. Marchese, L. Iuliano, M. Lombardi, and P. Fino, “Recent Progress in Beam-Based Metal Additive Manufacturing from a Materials Perspective: A Review of Patents,” *J. of Materi Eng and Perform*, vol. 30, no. 12, pp. 8689–8699, Dec. 2021, doi: 10.1007/s11665-021-06273-3.

2. A. Sharma *et al.*, “Machine Learning Based Parametric Optimization and Porosity Mapping in Selective Laser Melting of SS316L Alloy,” *J. of Materi Eng and Perform*, Aug. 2025, doi: 10.1007/s11665-025-11726-0.
3. D. Gu and Y. Shen, “Balling phenomena in direct laser sintering of stainless steel powder: Metallurgical mechanisms and control methods,” *Materials & Design*, vol. 30, no. 8, pp. 2903–2910, Sept. 2009, doi: 10.1016/j.matdes.2009.01.013.
4. I. Yadroitsev, A. Gusarov, I. Yadroitsava, and I. Smurov, “Single track formation in selective laser melting of metal powders,” *Journal of Materials Processing Technology*, vol. 210, no. 12, pp. 1624–1631, Sept. 2010, doi: 10.1016/j.jmatprotec.2010.05.010.
5. T. Yang *et al.*, “The influence of process parameters on vertical surface roughness of the AlSi10Mg parts fabricated by selective laser melting,” *Journal of Materials Processing Technology*, vol. 266, pp. 26–36, Apr. 2019, doi: 10.1016/j.jmatprotec.2018.10.015.
6. A. Charles, A. Elkaseer, U. Paggi, L. Thijs, V. Hagenmeyer, and S. Scholz, “Down-facing surfaces in laser powder bed fusion of Ti6Al4V: Effect of dross formation on dimensional accuracy and surface texture,” *Additive Manufacturing*, vol. 46, p. 102148, Oct. 2021, doi: 10.1016/j.addma.2021.102148.
7. P. Manikandan and K. Venkatesan, “Role of volumetric energy density on surface quality and mechanical properties of selective laser melted 310 stainless steel,” *Results in Engineering*, vol. 25, p. 104479, Mar. 2025, doi: 10.1016/j.rineng.2025.104479.
8. W. Abd-Elaziem, S. Elkatatny, T. A. Sebaey, M. A. Darwish, M. A. Abd El-Baky, and A. hamada, “Machine learning for advancing laser powder bed fusion of stainless steel,” *Journal of Materials Research and Technology*, vol. 30, pp. 4986–5016, May 2024, doi: 10.1016/j.jmrt.2024.04.130.
9. S. M. Yusuf, Y. Chen, R. Boardman, S. Yang, and N. Gao, “Investigation on Porosity and Microhardness of 316L Stainless Steel Fabricated by Selective Laser Melting,” *Metals*, vol. 7, no. 2, Art. no. 2, Feb. 2017, doi: 10.3390/met7020064
10. G. O. Barrionuevo, J. A. Ramos-Grez, X. Sánchez-Sánchez, D. Zapata-Hidalgo, J. L. Mullo, and S. D. Puma-Araujo, “Influence of the Processing Parameters on the Microstructure and Mechanical Properties of 316L Stainless Steel Fabricated by Laser Powder Bed Fusion,” *Journal of Manufacturing and Materials Processing*, vol. 8, no. 1, Art. no. 1, Feb. 2024, doi: 10.3390/jmmp8010035.
11. N. M. H. Alamri, M. Packianather, and S. Bigot, “Predicting the Porosity in Selective Laser Melting Parts Using Hybrid Regression Convolutional Neural Network,” *Applied Sciences*, vol. 12, no. 24, Art. no. 24, Jan. 2022, doi: 10.3390/app122412571.
12. A. E. Pandelea, “Image Processing Using Artificial Neural Networks,” *The Bulletin of the Polytechnic Institute of Jassy, Construction. Architecture Section*, Jan. 2015, Accessed: July 13, 2025. [Online]. Available: https://www.academia.edu/83637782/Image_Processing_Using_Artificial_Neural_Networks
13. D. Soler, M. Telleria, M. B. García-Blanco, E. Espinosa, M. Cuesta, and P. J. Arrazola, “Prediction of Surface Roughness of SLM Built Parts after Finishing Processes Using an Artificial Neural Network,” *JMMP*, vol. 6, no. 4, p. 82, Aug. 2022, doi: 10.3390/jmmp6040082.
14. M. S. Alam *et al.*, “Additively manufactured 316L stainless steel as a potential alternative implant material,” *Journal of Materials Research and Technology*, vol. 34, pp. 2358–2373, Jan. 2025, doi: 10.1016/j.jmrt.2024.12.199.
15. D. N. Aqilah, A. K. M. Sayuti, Y. Farazila, D. Y. Suleiman, M. A. N. Amirah, and W. B. W. N. Izzati, “Effects of Process Parameters on the Surface Roughness of Stainless

Steel 316L Parts Produced by Selective Laser Melting," *Journal of Testing and Evaluation*, vol. 46, no. 4, pp. 1673–1683, July 2018, doi: 10.1520/JTE20170140.